IEEE Photonics Journal
An IEEE Photonics Society Publication



# Experimental Study of Output Characteristics of Bi-Directional Pumping High Power Fiber Amplifier in Different Pumping Schemes

Volume 9, Number 3, June 2017

Chen Shi
Rong Tao Su
Han Wei Zhang
Bao Lai Yang
Xiao Lin Wang
Pu Zhou
Xiao Jun Xu
Qi Sheng Lu

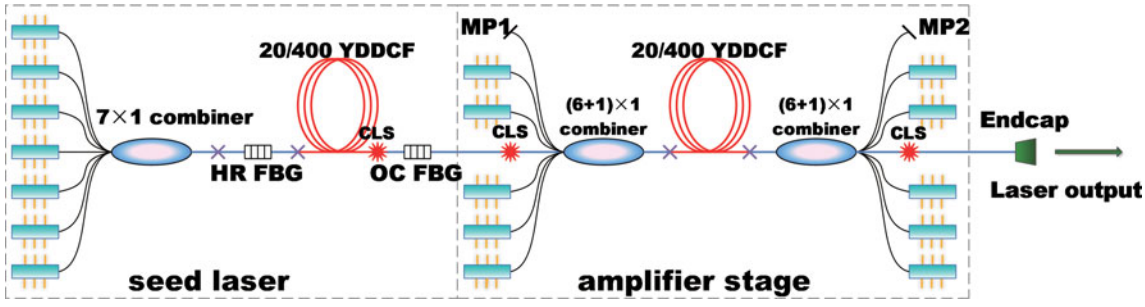


DOI: 10.1109/JPHOT.2017.2679753
1943-0655 © 2017 IEEE

# Experimental Study of Output Characteristics of Bi-Directional Pumping High Power Fiber Amplifier in Different Pumping Schemes

**Chen Shi, Rong Tao Su, Han Wei Zhang, Bao Lai Yang, Xiao Lin Wang, Pu Zhou, Xiao Jun Xu, and Qi Sheng Lu**

College of Optoelectronics Science and Engineering, National University of Defense Technology, Changsha, Hunan 410073, China

*DOI:10.1109/JPHOT.2017.2679753*


Manuscript received January 27, 2017; revised February 23, 2017; accepted March 6, 2017. Date of publication March 8, 2017; date of current version May 18, 2017. This work was supported in part by the National Natural Science Foundation of China under Grant 61505260 and in part by the National Key Research and Development Program of China under Grant 2016YFB0402204. Corresponding authors: C. Shi and X. L. Wang (email: bigbryant@nudt.edu.cn; chinawxllin@163.com).

**Abstract:** In this paper, we have constructed an all-fiberized bi-directional pumping fiber amplifier. The output time domain signals and limitations of copumping and counterpumping schemes were experimentally investigated. The power scaling of copumping and counterpumping scheme is restricted by stimulated Raman scattering (SRS) and transverse modal instability (TMI), respectively. The highest output power of 3.06 kW was achieved by using bi-directional pumping. Finally, we tested the relationship between SRS threshold and injected seed power.

**Index Terms:** Fiber lasers, fiber nonlinear optics, laser amplifiers.

## 1. Introduction

High average power lasers are needed for materials processing, medical treatment, and many other industrial applications. Over the past decade, output power of fiber lasers have experienced a rapidly boost with the development of large mode area (LMA) double-clad fibers and cladding pump technology [1]–[3]. Among them, ytterbium-doped fiber lasers and amplifiers at 1 $\mu$m have shown tremendous optical efficiency and have reached over 100 kW output power by combining tens of kW-level single mode fiber lasers. The power can be further scaled by increasing the power of single laser or by adding up the number of combined beams.

Compared with fiber laser oscillator, fiber amplifiers can offer the structure with simpler configuration and using fewer components to achieve higher output power more effectively and directly. However, after a rapid development of fiber laser technology in 21st century, further power scaling of near diffraction limit fiber laser has been blocked by several factors, such as optical damage, pump brightness, inelastic stimulated scattering (mainly SRS and stimulated Brillioun scattering (SBS)) [4], and a phenomenon that has become urgent in recent years: thermally induced TMI [5]–[8]. In wideband amplifiers, SRS and TMI are main limitations to achievable output power. To date, the methods of suppressing SRS effect are mainly focused on enlarging mode area [9], shorten fiber length or using special designed fibers [10]. The transverse modal instabilities are the

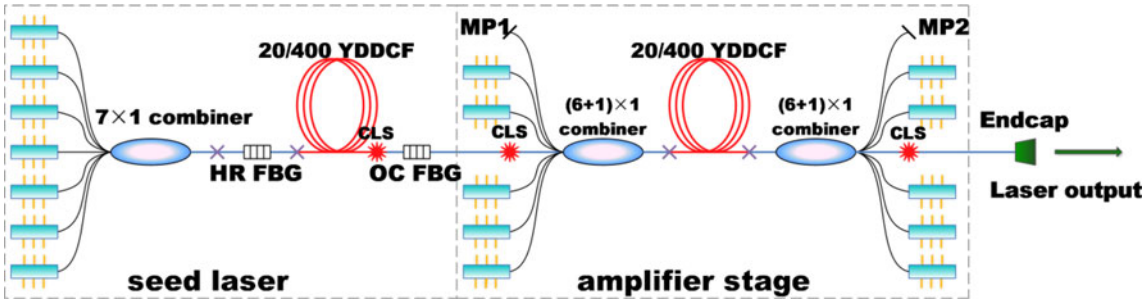


Fig. 1. Experimental configuration of high power bi-directional pumping amplifier.

temporal interplay between different transverse modes after a certain threshold power is reached in certain fiber amplifiers. Much theoretical and experimental research has studied and revealed the physical origin and phenomena of TMI [11]–[15], and TMI suppression is mainly realized using coiling or relatively low absorption pumping.

In this manuscript, we have constructed an all-fiberized bi-directional pumping fiber amplifier in order to balance SRS and TMI effect in our fiber amplifier. The output time domain signals and limitations of co-pumping and counter-pumping schemes were experimentally investigated. The power scaling of co-pumping and counter-pumping scheme are restricted by SRS and TMI, respectively. The highest output power of 3.06 kW was achieved using bi-directional pumping. Finally, we tested the relationship between SRS intensity and injected seed power.

## 2. Experimental Setup

The experimental configuration of our bi-directional pumping fiber amplifier is shown in Fig. 1. The seed laser of our system is a homemade all-fiber laser oscillator. Seven pump laser diodes (LDs) at 915 nm wavelength are combined by a $7 \times 1$ pump combiner and injected into the cavity through high reflective (HR) fiber Bragg grating (FGB). A pair of FBGs whose central reflective wavelengths are 1080 nm are used as cavity mirrors. The reflectivity of HR FBG is 99.9% while which of output-coupling (OC) FBG is 11%. A piece of $\sim$39 m long 20/400 ytterbium-doped double-clad fiber (YDDCF) is inserted between the FBG pair as gain medium. The cladding light stripper (CLS) is made between the splicing point between YDDCF and OC FBG to release the thermal pressure of OC FBG.

The output port of OC FBG is directly fused into the signal port of a $(6 + 1) \times 1$ combiner to provide seed power to the amplifier stage and the CLS is made at this point to avoid unabsorbed backward pump laser injection to the seed laser. The gain fiber of our amplifier is a piece of large mode area (LMA) YDDCF with 20 $\mu$m core and 400 $\mu$m inner-cladding. The numerical aperture (NA) of fiber core and inner clad are 0.06 and 0.46, respectively. The nominal core absorption coefficient to 976 nm wavelength is 1.44 dB/m. In our experiment, the active fiber length is chosen to be $\sim$19 m to ensure adequate total pump absorption and then shorten to $\sim$17.35 m in order to suppress SRS. Ten $\sim$500 W pump lasers which emit at 976 nm are coupled into active fiber through two $(6 + 1) \times 1$ combiners by forward and backward pumping direction, respectively. All the pump lasers in our experiment are working under CW regime. The amplified signal power is led out from the signal port of backward pumping combiner and a pigtailed endcap is spliced to the output port to eliminate probable harmful feedbacks at output facet. A CLS is also made before the connection point of endcap to provide protection to the endcap. The total length of passive fiber between endcap and output port of backward combiner is $\sim$9 m. After the endcap, we use a power meter, optical spectrum analyzer (OSA), and photonic detector (PD) to record power, optical spectrum and time domain data, respectively. Both the bandwidth of PD and oscilloscope are 1 GHz in our experiment. In the time trace measurement process, the PD with a pinhole with 1.5 mm diameter is

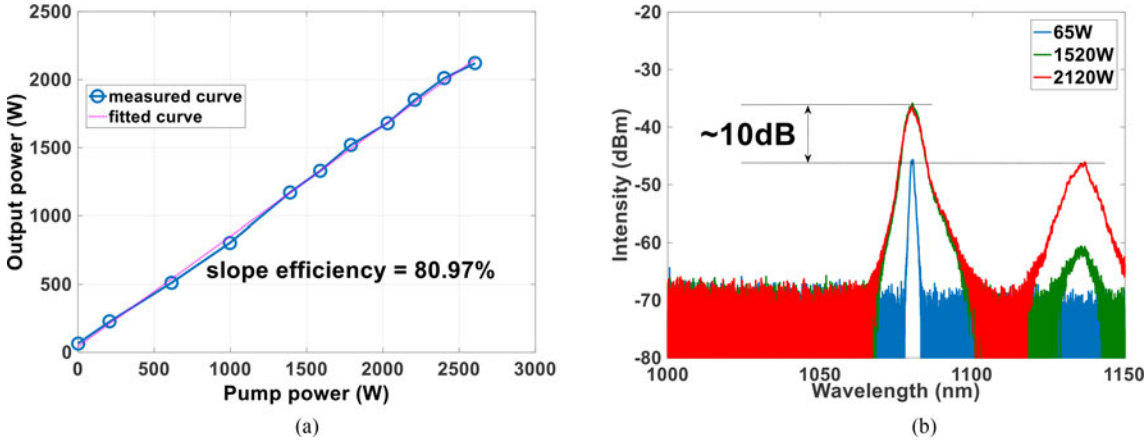


Fig. 2. Result of forward pumping scheme. (a) Output power versus pump power. (b) Optical spectra of different output powers.

put in the center of collimated beam to monitor the onset of TMI. From previous research, we know that the identification of the presence of TMI is the time domain fluctuation with frequency less than 5 kHz [16], [17], and this will also be used as the criterion in our experiment.

It is worth noting that we only used five ports for both $(6 + 1) \times 1$ combiners. The idle ports are angle cleaved and used as monitoring ports (MPs) and we define MP of forward pump combiner as MP1 and MP of backward pump combiner as MP2. We can estimate unabsorbed pump power of both directions through measuring power and optical spectrum from MPs and monitoring the working status of our amplifier. All the components of our fiber laser system are put on a water cooling plate to keep their temperatures fulfill appropriate working situations.

## 3. Experimental Results and Discussion

The seed light will propagate through our main amplifier stage. Because of that a fraction of seed power will lost by the absorption of active fiber, we will judge the seed power directly from the output port of our whole system. In this section, we firstly test the performance of our amplifier under co-pumping and counter-pumping scheme, respectively. Then, bi-directional pumping is employed to achieve further power scaling. Finally, the seed power is altered to investigate its influence on the SRS excitation on output spectra of the fiber amplifier.

### *3.1 Performance of Co-Pumping Scheme*

First, we test the performance of our fiber amplifier under forward pumping scheme. In this testing case, the length of active fiber is ~19 m. The seed power is fixed to be 65 W as its working point. Then the forward pumping LDs are turned on. The power variation curve and output spectra are plotted in Fig. 2.

As shown in Fig. 2(a), the output power is linearly increasing along with the increment of pump power. The overall slope efficiency of co-pumping scheme of our amplifier is 80.97%. The optical spectra of output power at 65 W (seed laser), 1520 W and 2120 W are depicted in Fig. 2(b). When the output power is below 1.5 kW, there is no obvious SRS that can be observed on the spectra data. After the output power reaches 1.5 kW, the Raman stokes component begin to appear and grow. Even though the appearance of SRS has no influence on the efficiency of our amplifier, the Raman stokes light is only ~10 dB below the intensity of signal light at 2.12 kW output power, and it surely restricts further power scaling in co-pumping scheme. As for the temporal characteristics, the time domain data has been plotted in Fig. 3(a).

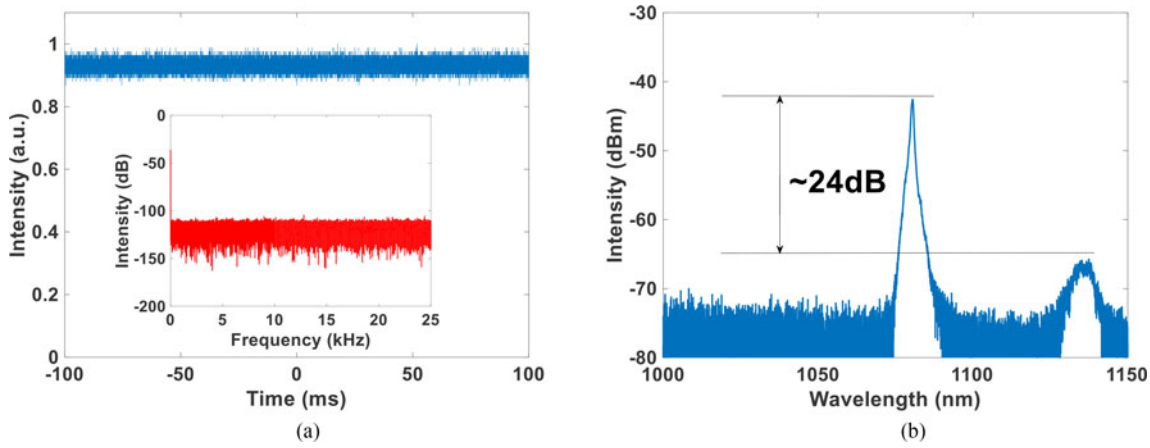


Fig. 3. (a) Temporal characteristics of co-pumping scheme at 2.12 kW output power. (Inset) Fourier transform of time series. (b) Measured spectrum from MP2 of co-pumping scheme at 2.12 kW output power.

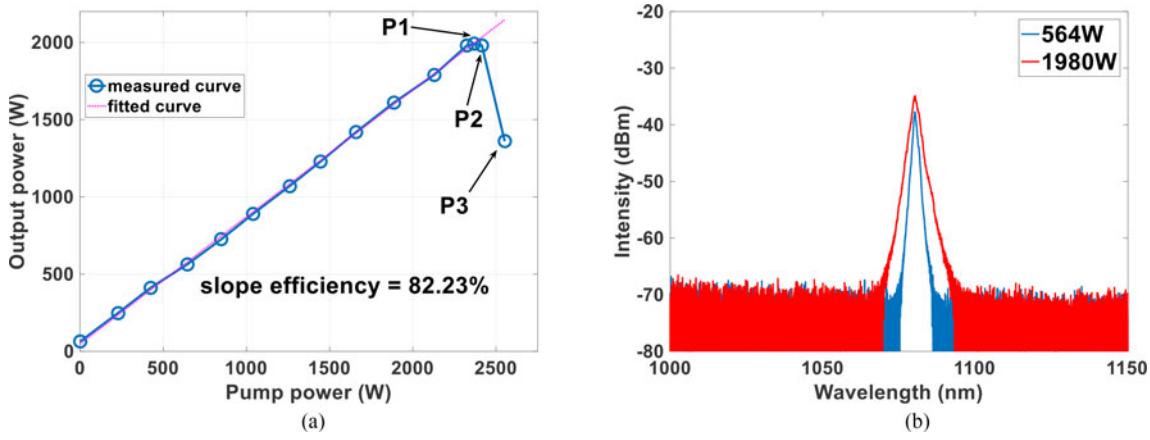


Fig. 4. Result of forward pumping scheme. (a) Output power versus pump power. (b) Optical spectra of different output powers.

As we can see from Fig. 3(a), the time series of output power is stable and there is no special frequency exists on the Fourier spectrum of the series, which shows the steady working status of co-pumping scheme of our fiber amplifier. Because of that passive fiber also contributes to SRS effect, we also measured the output spectrum from MP2 to consider the contribution of passive fibers between backward pumping combiner and endcap in SRS excitation. The measured spectrum is plotted in Fig. 3(b). The Raman stokes light can also be observed on Fig. 3(b) but is ∼14 dB weaker than which is measured at endcap. This result means that the passive fibers between backward pumping combiner and endcap contributes at least 10 dB of SRS excitations in this experimental configuration.

### *3.2 Performance of Counter-Pumping Scheme*

Compared with co-pumping scheme, the counter-pumping amplifier has totally different power variation trend and heat load distributions inside the active fiber. In order to compare with co-pumping case, the seed power in the counter-pumping scheme is also set to 65 W. The power variation curve and output spectra are plotted in Fig. 4.

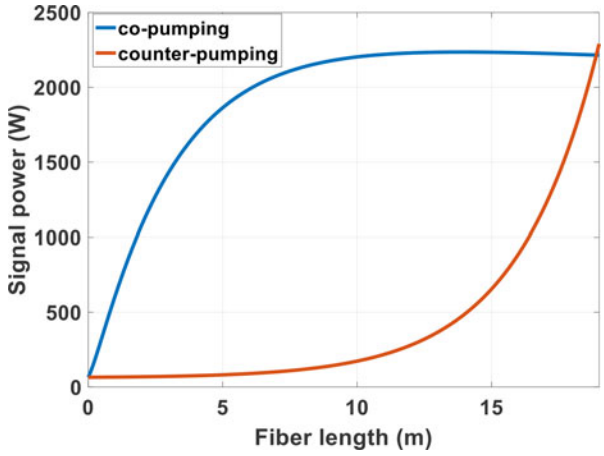


Fig. 5. Simulated signal variation curves in co- and counter-pumping schemes.

Unlike Fig. 2(b), the spectra curves from Fig. 4(b) are very clean, and there is only signal light shown on the picture which indicate counter-pumping scheme has higher SRS threshold than co-pumping scheme. In fact, this difference is induced by the different signal variation trends inside active fiber. By using the steady-state rate equation [18], we can simulate the variation curves of signal laser in both pumping schemes. Assume that the total pump powers are both 2.5 kW in both co- and counter-pumping scheme, the calculated curves are plotted in Fig. 5.

As we can see from Fig. 5, the average signal intensity in active fiber of co-pumping scheme is much higher than which in counter-pumping scheme. This kind of difference means that the counter-pumping has lower Raman pump intensity and shorter Raman interaction length than co-pumping scheme, which lead to higher SRS threshold.

Before the output power reaches 1.98 kW, the output power was increasing linearly with the increment of pump power and the slope efficiency was 82.23%. When we tried to further increase the pump power, we found that the increment of output power was stopped and even dropped a lot. The stationary or even drop-off of output power can obviously impute to thermally-induced TMI. To verify the occurrence of TMI, we measured the time domain signals after 1.98 kW output power (noted as P1, P2 and P3 on Fig. 4(a)), and they have been plotted in Fig. 5.

As we can see from Fig. 6(a), only slight fluctuations can be observed on curve P1 and P2, which correspond to the start-up of TMI. When the pump power reaches point P3, the periodic fluctuation will suddenly become violent. At the same time, the corresponding component of 2 kHz $\sim$ 3 kHz will appear on the Fourier spectra as shown in Fig. 6(b). We also observed the change on the CLS region because more light will leak out from CLS as long as TMI happens. In short, TMI is the main restriction of counter-pumping scheme power scaling in our fiber amplifier system.

When recalling the results of co-pumping scheme, we can see that the TMI threshold of counter-pumping is lower than co-pumping scheme in our experiment. There are two possible explanations for this. First, counter-pumping scheme will create larger temperature gradient in active fiber than co-pumping scheme because of stronger pump absorption at one end of active fiber. This kind of thermal imbalance will create thermally-induced refractive index grating more easily and lead to harder intermodal coupling [19]. In order to theoretically calculate and compare the longitudinal thermal pressure between co- and counter-pumping scheme, a verified model is used in this computational case [20]. The calculated temperature distributions and corresponding temperature gradients of active fiber in our experimental configuration under 2500 W co-pumping and counter-pumping have been shown in Fig. 7. We can see clearly that the maximum temperature gradient of co-pumping is at least two times higher than which of counter-pumping scheme and the highest temperature in fiber core in counter-pumping scheme is also higher than co-pumping scheme, which indicate possible higher intermodal coupling strength inside the active fiber.

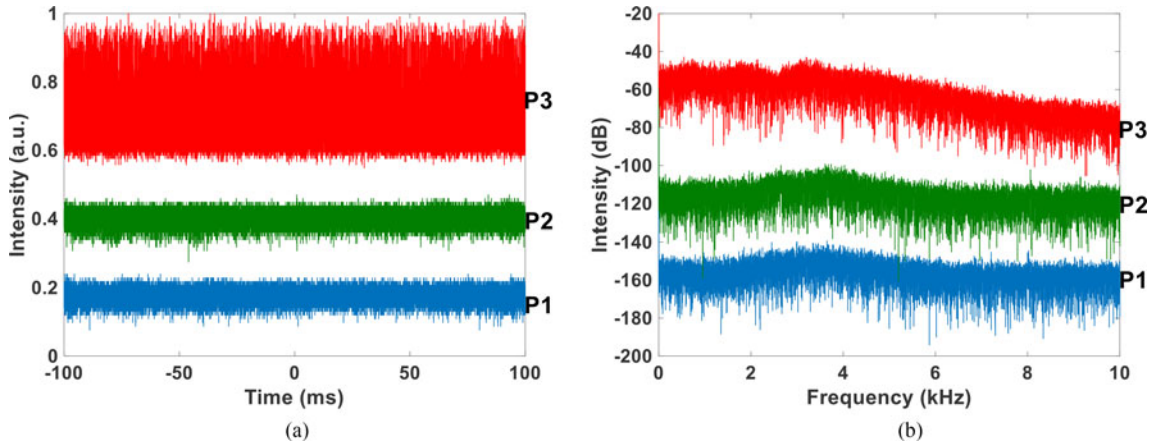


Fig. 6. (a) Temporal characteristics of co-pumping scheme at corresponding output power. (b) Fourier spectra of corresponding time series.

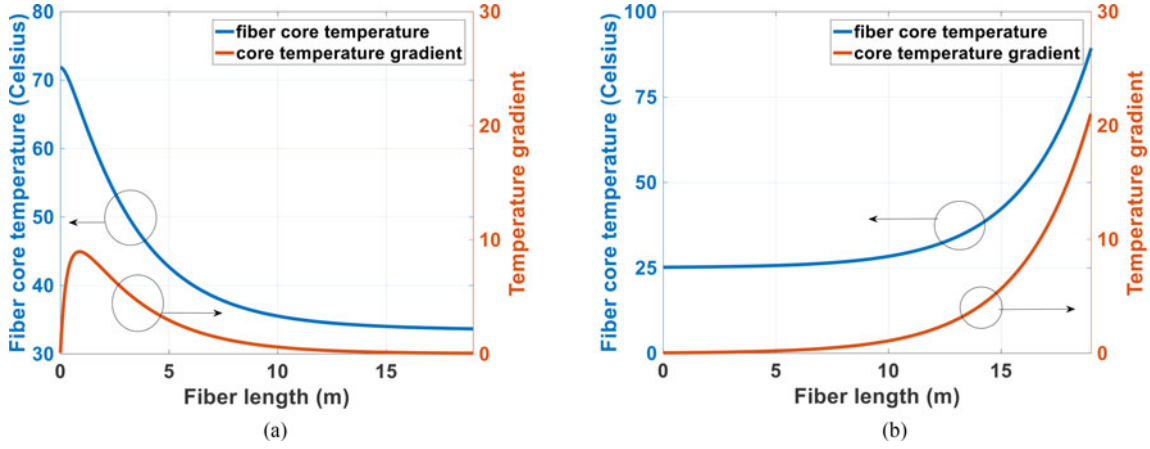


Fig. 7. (a) Calculated temperature distribution (blue) and temperature gradient (red) of 2500 W co-pumping scheme. (b) Calculated temperature distribution (blue) and temperature gradient (red) of 2500 W counter-pumping scheme.

Second, the part of active fiber that close to output port was coiled much looser than which close to the input port. It is well known that the curvature loss difference between $LP_{01}$ and $LP_{11}$ modes is sensitive to the curvature radius, which means smaller coiling radius will have better performance in suppressing TMI and increase TMI threshold [21]. The curvature loss difference of active fiber in our experiment is theoretically calculated and plotted in Fig. 8. This result indicates that the curvature loss of higher-order-modes (HOMs) at port close to forward pump injection is much higher than which close to backward pump injection, which means HOMs can be better suppressed in co-pumping scheme and the TMI threshold will be higher correspondingly.

Overall, based on the experimental configuration, the co-pumping was limited by SRS while counter-pumping was limited by TMI. Therefore, in the next step, bi-directional pumping scheme is employed in order to balance SRS and TMI and then realize further power scaling in our experiment.

### *3.3 Performance of Bi-Directional Pumping*

On the base of previous tests, we now have idea that forward and backward pumping scheme both have their own limitations (SRS and TMI, respectively). In this part, we will limit backward pump

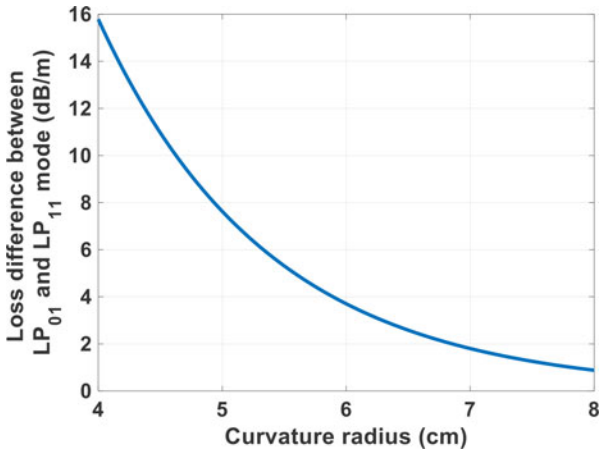


Fig. 8. Calculated curvature loss difference between $L\,P_{01}$ and $L\,P_{11}$ mode of 20/400, NA $=$ 0.06 fiber.

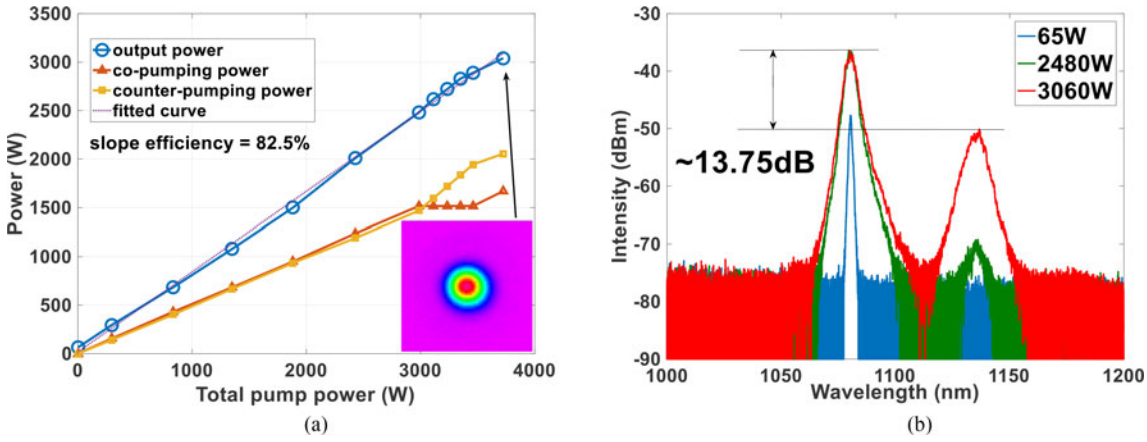


Fig. 9. Result of bi-directional pumping scheme. (a) Output power, co-pumping power and counter-pumping power versus total pump power. (Inset) Measured beam pattern at 3.06 kW output power. (b) Optical spectra of different output powers.

power below 2.1 kW to avoid possible TMI effect. At the same time, the length of active fiber is shortened to ∼17.35 m to suppress SRS effect. The seed power will keep as 65 W. The power variation curve and output spectra are plotted in Fig. 9.

Our strategy is to increase pump powers from both directions at beginning and observing the real-time measured spectrum from OSA. After SRS is observed, only counter-pumping power is further increased. When counter-pumping power is near 2.1 kW, co-pumping power can be slightly increased a little. The detailed pumping power variation and output power curve are plotted in Fig. 9(a). Using this method, the highest output power of 3.06 kW is achieved. The overall slope efficiency is 82.5%. The output beam at highest output power has also been measured and shown in the inset of Fig. 9(a), and the measured $M^2$ factor is 1.28. Fig. 9(b) shows the measured spectra of seed laser, output power of 2.48 kW and 3.06 kW, respectively. The Raman stokes light is ∼13.75 dB below signal light at 3.06 kW output power. Also, the time domain signal and optical spectrum from MP2 are also obtained and depicted in Fig. 10.

The temporal signal and its Fourier spectrum in Fig. 10(a) are all clean, which indicates successful TMI prevention. The measured optical spectrum from MP2 in Fig. 10(b) is also SRS free, which means the SRS components in Fig. 9(b) are all induced by passive fibers. This result

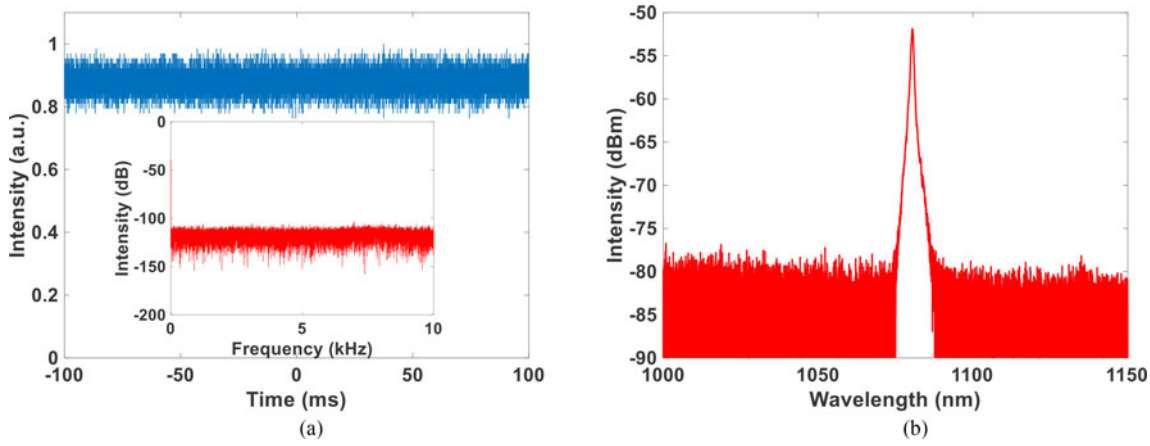


Fig. 10. (a) Temporal characteristics of bi-directional pumping scheme at 3.06 kW output power. (Inset) Fourier transform of time series. (b) Measured spectrum from MP2 of bi-directional pumping scheme at 3.06 kW output power.

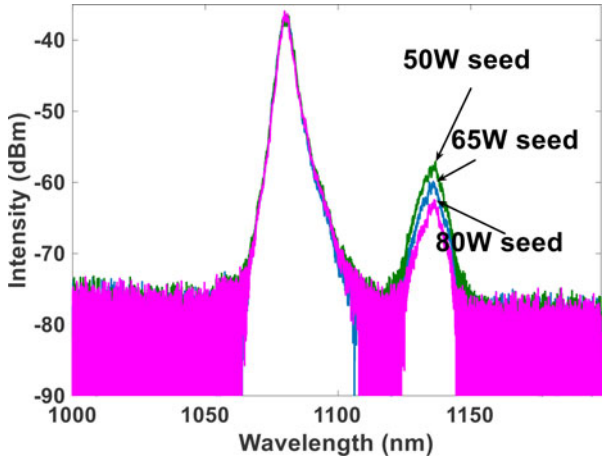


Fig. 11. Output spectra of ~2.7 kW output with 50 W, 65 W, and 80 W seed power injection.

reveals the potential of bi-directional pumping method in balancing SRS and TMI in wideband laser amplification.

### *3.4 SRS Intensities for Different Seed Power Injection*

In this part, we alter the seed power to investigate the SRS intensities under different seed power injection. Three seed powers are used in this testing case, 50 W, 65 W and 80 W. The different seed powers are all injected into amplifier and amplified to ~2.7 kW using the same pumping configuration. The optical spectra are depicted in Fig. 11.

From Fig. 11, we can see that the SRS threshold is increasing with the increment of seed power. It is very interesting that we found that we had a totally opposite conclusion with previous experiments [22]. The result in [22] showed that in a higher seed power level ($10^2 \sim 10^3$ W magnitude), the SRS threshold will decrease with the increment of seed power. This confliction reminds us there should be a best seed power to every specific fiber amplifier. With the best seed power injection, the fiber amplifier could obtain the highest SRS threshold than any other seed power. The theoretical

prediction has already been made by the researchers of National University of Defense Technology [23].

## 4. Conclusion

In this manuscript, we have constructed an all-fiberized bi-directional pumping fiber amplifier. The output characteristics and limitations of co-pumping and counter-pumping schemes were experimentally investigated. We found that, in our experimental configuration, the power scaling of co-pumping scheme is mainly restricted by SRS, while counter-pumping scheme is mainly limited by thermally-induced TMI. Then, bi-directional pumping scheme was employed and successfully balanced SRS and TMI. The highest output power of 3.06 kW was achieved using bi-directional pumping. Finally, we tested the relationship between SRS threshold and injected seed power and figure out there might be a best seed power for every specific fiber amplifier that can make it has the highest SRS threshold.

## Acknowledgment

The authors would like to thank K. Zhang, X. Xu, L. Chen, S. Liu, Y. Liu, and Y. Luo for their help and discussions about our experiments.

## References

[1] M. N. Zervas and C. A. Codemard, "High power fiber lasers: A review," *IEEE J. Select. Topics Quantum Electron.*, vol. 20, no. 5, pp. 219–241, Sep./Oct. 2014.
[2] D. J. Richardson, J. Nilsson, and W. A. Clarkson, "High power fiber lasers: Current status and future perspectives [Invited]," *J. Opt. Soc. Amer. B*, vol. 27, pp. B63–B92, 2010.
[3] O. G. Okhotnikov, *Fiber Lasers*. New York, NY, USA: Wiley, 2012.
[4] J. W. Dawson *et al.*, "Analysis of the scalability of diffraction-limited fiber lasers and amplifiers to high average power," *Opt. Exp.*, vol. 16, pp. 13240–13266, 2008.
[5] K. R. Hansen, T. T. Alkeskjold, J. Broeng, and J. Lægsgaard, "Thermally induced mode coupling in rare-earth doped fiber amplifiers," *Op. Lett.*, vol. 37, pp. 2382–2384, 2012.
[6] A. V. Smith and J. J. Smith, "Steady-periodic method for modeling mode instability in fiber amplifiers," *Opt. Exp.*, vol. 21, pp. 2606–2623, 2013.
[7] A. V. Smith and J. J. Smith, "Overview of a steady-periodic model of modal instability in fiber amplifiers," *IEEE J. Select. Topics Quantum Electron.*, vol. 20, no. 5, pp. 472–483, Sep./Oct. 2014.
[8] M. Kuznetsov, O. Vershinin, V. Tyrtyshnyy, and O. Antipov, "Low-threshold mode instability in $Yb^{3+}$-doped few-mode fiber amplifiers," *Opt. Exp.*, vol. 22, pp. 29714–29725, 2014.
[9] F. Kong *et al.*, "Ytterbium-doped 30/400 LMA fibers with a record-low ~NA of 0.028," in *Proc. Conf. Lasers Electro-Opt.,* San Jose, CA, USA, 2016, Paper SM2Q.2.
[10] J. Kim, P. Dupriez, C. Codemard, J. Nilsson, and J. K. Sahu, "Suppression of stimulated Raman scattering in a high power Yb-doped fiber amplifier using a W-type core with fundamental mode cut-off," *Opt. Exp.*, vol. 14, pp. 5103–5113, 2006.
[11] K. Hejaj *et al.*, "Controlling mode instability in a 500 W ytterbium-doped fiber laser," *Laser Phys.*, vol. 24, 2014, Art. no. 025102.
[12] K. R. Hansen and J. Lægsgaard, "Impact of gain saturation on the mode instability threshold in high-power fiber amplifiers," *Opt. Exp.*, vol. 22, pp. 11267–11278, 2014.
[13] H. Otto, N. Modsching, C. Jauregui, J. Limpert, and A. Tünnermann, "Impact of photodarkening on the mode instability threshold," *Opt. Exp.*, vol. 23, pp. 15265–15277, 2015.
[14] R. Tao, P. Ma, X. Wang, P. Zhou, and Z. Liu, "Influence of core NA on thermal-induced mode instabilities in high power fiber amplifiers," *Laser Phys. Lett.*, vol. 12, Art. no. 085101, 2015-01-01 2015.
[15] C. Jauregui, H. Otto, S. Breitkopf, J. Limpert, and A. Tünnermann, "Optimizing high-power Yb-doped fiber amplifier systems in the presence of transverse mode instabilities," *Opt. Exp.*, vol. 24, pp. 7879–7892, 2016.
[16] R. Tao, P. Ma, X. Wang, P. Zhou, and Z. Liu, "1.3 kW monolithic linearly polarized single-mode master oscillator power amplifier and strategies for mitigating mode instabilities," *Photon. Res.*, vol. 3, pp. 86–93, 2015.
[17] H. Otto *et al.*, "Temporal dynamics of mode instabilities in high-power fiber lasers and amplifiers," *Opt. Exp.*, vol. 20, pp. 15710–15722, 2012.
[18] Z. Zhang *et al.*, "Numerical analysis of stimulated inelastic scatterings in ytterbium-doped double-clad fiber amplifier with multi-ns-duration and multi-hundred-kW peak-power output," *Opt. Commun.*, vol. 282, pp. 1186–1190, 2009.
[19] C. Jauregui *et al.*, "Physical origin of mode instabilities in high-power fiber laser systems," *Opt. Exp.*, vol. 20, pp. 12912–12925, 2012.
[20] D. C. Brown and H. J. Hoffman, "Thermal, stress, and thermo-optic effects in high average power double-clad silica fiber lasers," *IEEE J. Quantum Electron.*, vol. 37, no. 2, pp. 207–217, Feb. 2001.

[21] R. Tao, R. Su, P. Ma, X. Wang, and P. Zhu, "Suppressing mode instabilities by optimizing the fiber coiling methods," *Laser Phys. Lett.*, vol. 14, 2017, Art. no. 025101.
[22] J. Wang, D. Yan, S. Xiong, B. Huang, and C. Li, "High power all-fiber amplifier with different seed power injection," *Opt. Exp.*, vol. 24, pp. 14463–14469, 2016.
[23] W. Liu, P. Ma, H. Lv, J. Xu, P. Zhou, and Z. Jiang, "General analysis of SRS-limited high-power fiber lasers and design strategy," *Opt. Exp.*, vol. 24, pp. 26715–26721, 2016.